Indones. J. Chem., 2023, 23 (2), 285 - 297

285

Activity and Selectivity of Mesoporous Silica Catalyst for Hydrocracking Process of Used Palm Oil into Biogasoline

Ahmad Suseno[1], Karna Wijaya[2*], Edy Heraldy[3], Lukman Hakim[4], Wahyu Dita Saputri[5], and Gunawan Gunawan[1]

[1]*Department of Chemistry, Faculty of Sciences and Mathematics, Diponegoro University, Jl. Prof. H. Soedarto, S.H., Tembalang, Semarang 50275, Indonesia*

[2]*Department of Chemistry, Faculty of Mathematics and Natural Sciences, Universitas Gadjah Mada, Sekip Utara, Yogyakarta 55281, Indonesia*

[3]*Department of Chemistry, Faculty of Mathematics and Natural Sciences, Universitas Sebelas Maret, Jl. Ir. Sutami 36A, Surakarta 57126, Indonesia*

[4]*Department of Chemistry, Faculty of Mathematics and Natural Sciences, Brawijaya University, Jl. Veteran, Malang 65145, Indonesia*

[5]*Research Center for Quantum Physics, National Research and Innovation Agency (BRIN), Habibie Science and Technology Complex (Puspiptek), Serpong 15314, South Tangerang, Indonesia*

Abstract: *Research on the synthesis of mesoporous silica catalyst, as well as its activity and selectivity in the hydrocracking of used palm oil, has been carried out. The research involved the preparation of mesoporous silica catalyst by varying the volume ratio of TEOS:CTAB at 2:1, 4:1, and 8:1, then calcined at 500 °C. Synthesis success was confirmed by FTIR, XRD, SEM-EDX, GSA, and hydrocracking selectivity by GC-MS analysis. The results showed that the more TEOS added, the silica bond composition, crystallinity, pore size, and product selectivity increased. The best catalyst performance was obtained from a TEOS:CTAB ratio of 8:1 at a calcination temperature of 500 °C (MCT81-500), which indicated the presence of Si-OH and Si-O-Si groups with a Si percentage of 45.31%, pore size diameter of 31.912 nm, and a total pore volume of 0.040 cc/g. In addition, the application of MCT81-500 in the hydrocracking process of used palm oil can produce a bio-gasoline (C5-C12) and kerosene (C12-C15) of 92.24 and 7.76 wt.%, respectively. This study shows that mesoporous silica has good potential for catalytic activity to convert used cooking oil waste into an environmentally friendly energy source.*

Keywords: *mesoporous silica; hydrocracking; palm oil; biogasoline*

■ INTRODUCTION

For several years, fossil fuels have been widely used in various aspects of life. However, this fuel is non-renewable and will eventually run out. Various studies on alternative fuel sources to overcome the problem of fossil fuels have been carried out [1]. Biogasoline is like fossil fuels in terms of functionality and clean combustion [2-3]. Used palm oil is an alternative source of biogasoline. Used palm oil is produced mostly by households, the food industry, and fast-food restaurants. Used palm oil consists of long hydrocarbon chains, such as fatty acids, triglycerides, and their derivatives which can be converted into biogasoline. Therefore, the hydrocracking process is very necessary for converting used palm oil into fuel [4-5].

Mesoporous silica nanoparticles have attracted attention in various applications such as separation [6], catalysis [7], chemical sensing [8], and biomedicine [9]. Mesoporous silica has been synthesized in many previous studies showing various shapes or

morphologies, including monoliths, spheres, rods, films, and fibers [10-18]. They display promising functions for catalytic, electronic, separation, electrochemical, and optical applications [19-20]. In addition, the development of nanostructured materials is increasingly attracting interest in various application fields, including catalysis and adsorption. Thermal and hydrothermal stabilities are also important parameters to be considered when designing materials for heterogeneous catalytic reaction applications. The type of heterogeneous catalyst currently being studied is a silica-based catalyst. This type of catalyst has some advantages, namely surface reactivity, good chemical and thermal resistance and acidity, which is easily modified by the hydrocracking process [21].

Hydrocracking is one of the important processes in petroleum processing. In the hydrocracking process, hydrocarbon compounds break down into small-chain hydrocarbons such as gasoline, diesel, and kerosene fractions [22-23]. Development with the addition of a catalyst can speed up the hydrocracking process. Based on previous studies, it is known that hydrocracking catalysts with mesoporous dimension silica can increase the liquid yield [24]. Silica-based catalysts have surface reactive properties, good thermal, chemical, and acid resistance, and are easy to modify [25]. The nature of the silica catalyst is determined by several synthesis parameters, such as calcination temperature, solution pH, method of preparation, and precursor concentration [26]. In addition, a modification that can be made to increase the reactivity of silica is by forming mesopores. A pore is considered a mesopore when it has a pore size of 2 to 50 nm [27]. Mesoporous materials are very encouraging for hydrocracking processes due to their large surface area, thermal, chemical, and mechanical stability, regular pore distribution, and high adsorption capacity [24,28]. So, the development of mesoporous silica synthesis becomes important.

Mesoporous silica synthesis requires a silica source and a template. The most used silica sources are tetraethyl orthosilicate (TEOS) or sodium silicate, while cationic organic compounds such as cetyltrimethylammonium bromide (CTAB) are used as molds [29-30]. The type of template and the ratio of precursors used determine the size and distribution of mesoporous silica materials [24,31] as catalysts for hydrocracking [32-36]. Therefore, this study observed the activity and selectivity of mesoporous silica catalysts for the hydrocracking process of used palm oil into biogasoline. The effect of TEOS:CTAB composition variations were observed by characterization with FTIR, XRD, SEM-EDX, GSA, and hydrocracking selectivity with GC-MS to obtain the optimum catalyst performance ratio. In addition, this research is also expected to be a solution to the potential use of used cooking oil that is not utilized as an environmentally friendly energy source.

■ EXPERIMENTAL SECTION

Materials

The materials used in this study consisted of CTAB, TEOS, ammonium hydroxide (NH_4OH), and sodium hydroxide (NaOH) obtained from E. Merck. Palm oil was purchased from a traditional market in Semarang, Central Java. Hydrogen and nitrogen gases were obtained from PT. Samator Gas (Semarang, Central Java).

Instrumentation

The equipment and instruments used in this study included laboratory glassware, magnetic stirrers, ovens (Kirin), filter paper (Whatman no. 42), Gas Sorption Analyzers (GSA, Quantachrome Nova 1200e), Scanning Electron Microscope (SEM, Phenom ProX G6 desktop), X-ray Diffractometer (XRD, X'Pert3 Powder), Fourier Transform Infra-Red Spectrometer (FTIR, PerkinElmer Spectrum 100), and Gas Chromatography-Mass Spectrometry (GC-MS, GC-2010 Shimadzu).

Procedure

Preparation

An outline of the production scheme for mesoporous silica (MCT) as a catalyst for hydrocracking palm oil is shown in Fig. 1. Synthesis of mesoporous silica was performed by mixing 0.8018 g CTAB and 2, 4 and 8 mL TEOS separately. Then, the synthesis results are labeled as MCT21-500, MCT41-500, and MCT81-500. The mixture was stirred for 15 min. Then 5 mL of 2 M NaOH solution was added dropwise and continued
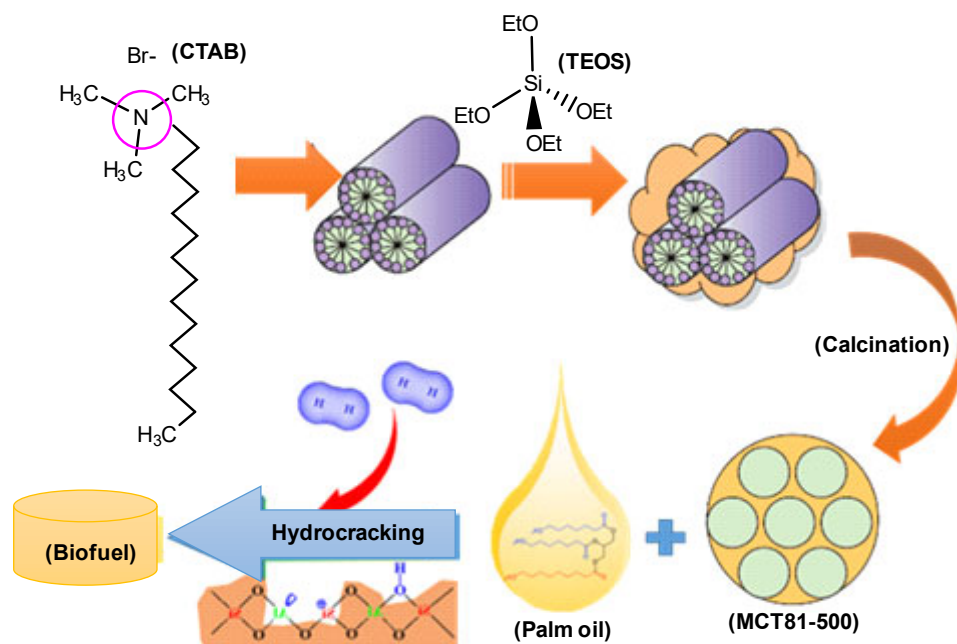
Indones. J. Chem., 2023, 23 (2), 285 - 297

287

Fig 1. Schematic illustration for the synthesis of MCT catalyst for hydrocracking palm oil

with stirring for 3 h at 80 °C. The solids obtained were filtered and washed with distilled water at neutral pH conditions. After that, drying was done at 150 °C for 2 h and followed by grinding and sifting at a size of 200 mesh. The final step was the calcination process in an open stainless reactor at 500 °C for 4 h in an inert N_2 atmosphere at 2 °C/min and then let it cool down to reach room temperature.

Characterization

The synthesis success of the mesoporous silica catalyst was analyzed by FTIR to confirm the functional groups, and the diffraction patterns were measured using the X'Pert3 Powder XRD in continuous scanning mode with a scan range of 1–10° and a scanning interval of 0.02°. In addition, morphology and pore size observations were carried out by using SEM and gas sorption analyzers while GC-MS was used to determine the effectiveness and composition of hydrocracking products.

Catalytic activity

The catalyst activity was observed in the hydrocracking process of used palm oil samples in a flex-bed microreactor system, as shown in Fig. 2. The catalyst was fed into the microreactor system with a weight ratio of catalyst/used palm oil of 1:100 (w/w). The used oil sample
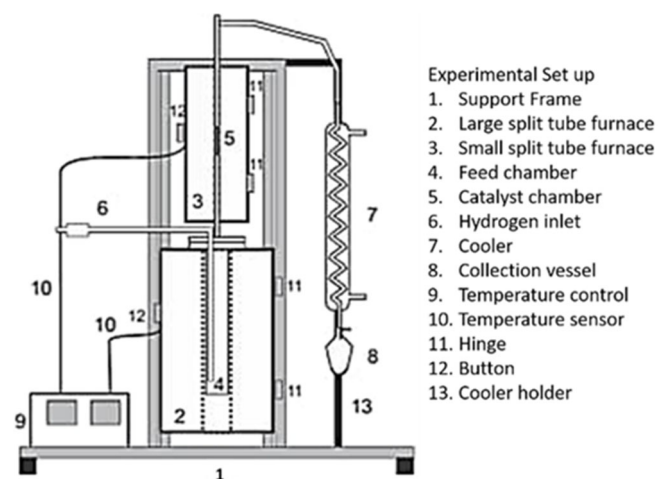

Experimental Set up
1. Support Frame
2. Large split tube furnace
3. Small split tube furnace
4. Feed chamber
5. Catalyst chamber
6. Hydrogen inlet
7. Cooler
8. Collection vessel
9. Temperature control
10. Temperature sensor
11. Hinge
12. Button
13. Cooler holder

Fig 2. Schematic of a hydrocracking microreactor

was put into the chamber feed and then heated until it evaporated. Simultaneously, the catalyst reactor was heated at 500 °C. Then H_2 gas was flowed into the feed chamber at a speed of 20 mL/min. Oil vapor entered the catalyst reactor containing mesoporous silica catalyst (MCT21-500, MCT41-500, and MCT81-500), and a hydrocracking reaction occurred. Furthermore, the product was cooled in a cool trap and collected in a container. Finally, the products obtained were analyzed using GC-MS. The chromatogram showed the relative percentage for each compound contained in the liquid

product. The selectivity of the catalyst in the hydrocracking reaction was measured from the peak area of the GC-MS chromatogram of each fraction. The conversion of feed to yield was calculated by using the following equations [32]:

$$\text{Liquid yield(wt.\%)} = \frac{W_{LP}}{W_F} \times 100\%$$

$$\text{Solid yield(wt.\%)} = \frac{W_R + \left(W_{UC} - W_{FC}\right)}{W_F} \times 100\%$$

$$\text{Gas product(wt.\%)} = 100\% - \text{wt.\%(liquid} - \text{solid)}$$

Selectivity of liquid yield

$$= \frac{\%\ \text{area GCMS fraction}\ C_x - C_y}{\%\ \text{total area GCMS}} \times 100\%$$

where, W_{LP}: weight of liquid product, W_F: weight of feed, W_R: weight of residue, W_{FC}: weight of fresh catalyst, and W_{UC}: weight of used catalyst

■ RESULTS AND DISCUSSION

The results of the infrared analysis of mesoporous silica material (MCT81-500) are shown in the spectra of Fig. 3. This analysis was carried out to determine the absorption resulted by the synthesized mesoporous silica and to observe changes in absorption after the adsorption of ammonia by mesoporous silica catalysts with a volume ratio of TEOS:CTAB = 8:1. Fig. 3(a) shows the initial spectra consisting of absorption of functional groups from Si–O–Si bending vibrations, symmetric Si–O–Si stretching vibrations, Si–OH stretching vibrations, asymmetric Si–O–Si stretching vibrations, H–O–H bending vibrations, Brønsted acid sites, and O–H stretching vibrations were observed to occur at wavenumbers 455, 794–802, 956–964, 1082–1087, 1635–1640 and 3465–3434 cm^{-1}, respectively. Then in Fig. 3(b) a new absorption peak appears at 1388 cm^{-1}, which shows an ammonia adsorption vibration band indicating the presence of Lewis acid and a combination of all acid sites. Ammonia is adsorbed on top of the sample at Lewis acid sites forming ammonium ions in the silica structure. The results of this study indicate that the adsorption of ammonia by MCT81-500 was carried out successfully through the acidic active site.

MCT catalyst crystallinity was analyzed by XRD to produce a diffractogram as shown in Fig. 4. The analysis

was carried out at 2θ = 2–15° with MCT samples of CTAB:TEOS variations (2:1; 4:1; and 8:1). The diffractograms of all samples after calcination showed indexable peaks at 100, at angles 2θ 2.61°, 3.02°, and 2.67° for MCT21-500, MCT41-500, and MCT81-500 materials, respectively.

The results showed that the CTAB:TEOS ratio variation produced a different crystallinity from the MCT81-500 sample, which resulted the highest crystallinity degree. Peak intensity increases with increasing silica content or TEOS/matrix ratio. The results
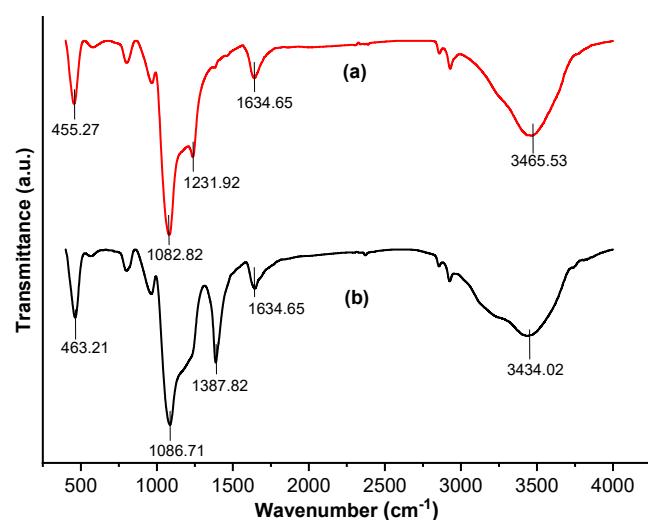

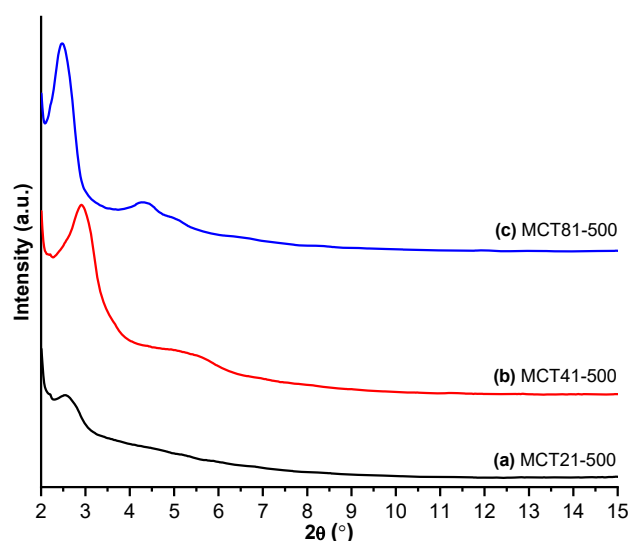**Fig 3.** FTIR spectra of MCT81-500: (a) before and (b) after adsorption of ammonia

Fig 4. XRD patterns of the mesoporous silica materials: (a) MCT21-500, (b) MCT41-500, and (c) MCT81-500
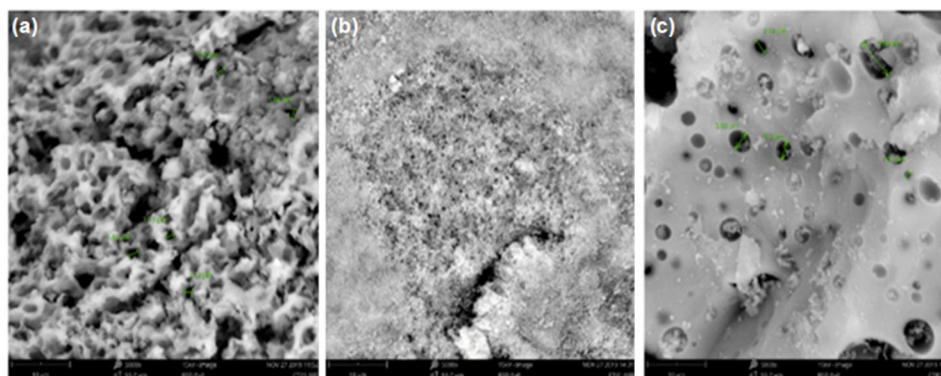
Fig 5. SEM images of (a) MCT21-500, (b) MCT41-500, and (c) MCT81-500

reflect that the composition of the precursor and surfactant significantly affects the morphology and crystallinity of the resulting mesoporous silica. These results also show whether the addition of a suitable matrix can improve the intensity of silica crystallinity based on SEM analysis.

Characterization of the catalyst morphology to determine the surface topography was carried out by SEM while the elemental composition on the surface of the catalyst was carried out by EDX. The SEM results in Fig. 5 illustrate that the variations in the TEOS:CTAB ratio affect many properties, such as pore size, surface area, and morphology. SEM images of the samples also show non-uniform particle sizes. This shows that CTAB as a mesoporous matrix agent has a wide range of molecular weight distribution. As shown in Fig. 5(a), (b), and (c), the surface morphology of the silica samples tends to be round and most of the particles tend to form bonds or large spherical particle pieces which are commonly known as clustering.

The results of the EDX analysis showed that the elemental content in Table 1 concluded that higher crystallinity was associated with an increase in silicate content. These results also conclude that higher crystallinity is consistent with higher silica

concentrations. Where in this result, the highest crystallinity structure was obtained from the synthesis of hierarchical mesoporous silica with a ratio of 8:1.

In the EDX analysis, the elements silica (Si), oxygen (O), carbon (C), and nitrogen (N) appear. Specifically, O and Si elements show the formation of silanol (Si–OH) and siloxane (Si–O–Si) groups. in addition, the appearance of certain carbon content in the MCT81-500 material confirms the XRD peak ($2\theta = 2.61°$) shown in Fig. 4.

Analysis of catalyst properties such as average diameter, pore distribution, total pore volume, and specific surface area was carried out by GSA. The results of the porous properties of the mesoporous silica catalyst are presented in Table 2.

The GSA analysis showed that the largest average pore radius was obtained with the MCT81-500 sample. This indicates that a larger radius of porous silica can be

Table 1. Elemental analysis results measured using EDX

Sample	Content (%)			
	Si	O	N	C
MCT21-500	27.50	64.24	8.26	-
MCT41-500	35.76	55.83	8.41	-
MCT81-500	45.31	41.11	6.02	7.75

Table 2. Pore properties of the mesoporous silica catalysts

Sample	Specific surface area (m²/g)	Total pore volume (cc/g)	Average pore diameter (nm)
MCT21-500	324.254	0.109	31.484
MCT41-500	382.514	0.199	31.892
MCT81-500	292.294	0.040	31.912

achieved by adding a minimal proportion of CTAB, especially in TEOS (silicon) precursors with a mold ratio of 8:1. However, other parameters such as specific surface area and total pore volume of MCT81-500 catalyst were the lowest. The increase and decrease in surface area are followed by the pore diameter. The pore diameter shows the highest pore distribution. The increased pore size does not slow down the process of diffusion of triglycerides into the catalyst. This ensures an optimal cracking process.

The adsorption isotherm of mesoporous silica is shown in Fig. 6. The isotherm pattern of mesoporous silica follows the type IV adsorption pattern. The type IV isotherm diagram shows four types of hysteresis loops which describe the mesoporous character of the intrinsic pore dimensions of the material [37-38]. To see the pore state more accurately, it is necessary to analyze the pore distribution curve in the material. The pore radius distribution data is shown in Fig. 7. The data shows the pore distribution according to mesoporous materials which have a sensitivity range of 2 to 50 nm.

The catalytic activity of MCT21-500, MCT41-500, and MCT81-500 was observed in the hydrocracking process of used palm oil. The product composition was analyzed by GC-MS to obtain a chromatogram like the example shown in Fig. 8. Fig. 8 shows the chromatogram of hydrocracking products with MCT81-500 catalyst, which produces different peaks according to their respective retention times. Hydrocracking products are differentiated due to differences in boiling points based
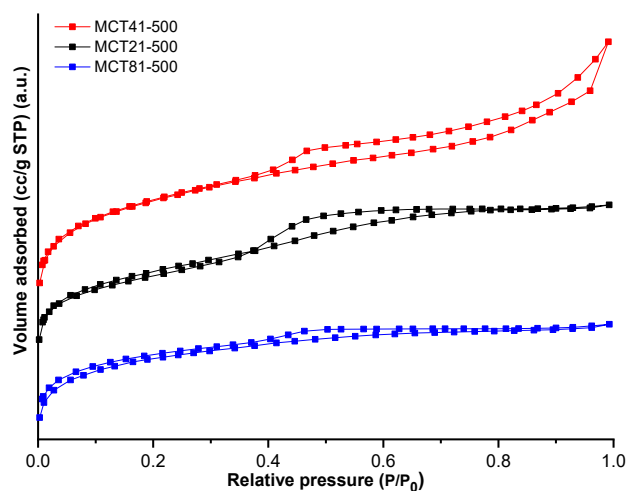

Fig 6. Adsorption-desorption isotherm curves of the mesoporous silica materials
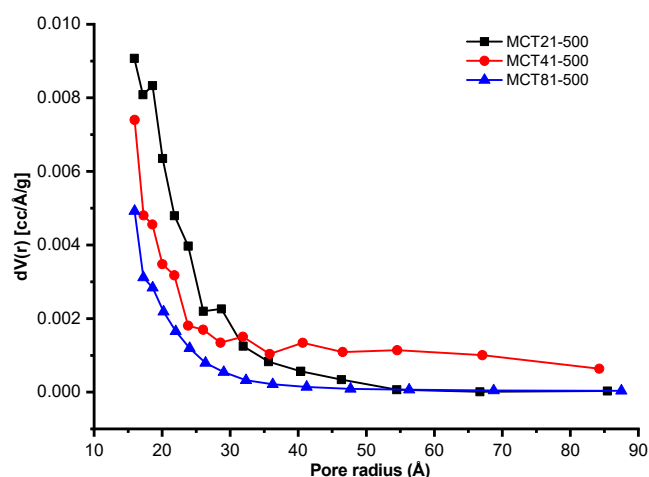

Fig 7. Pore radius size distribution of the mesoporous silica materials
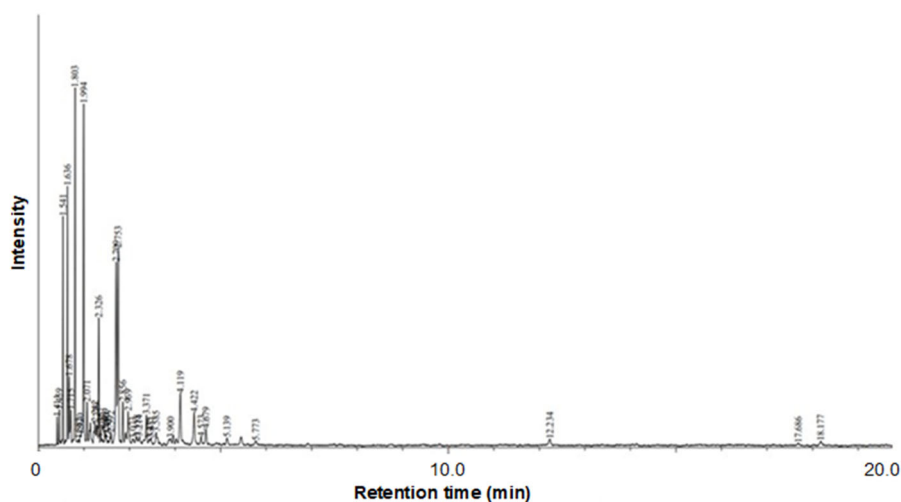

Fig 8. GC-MS chromatogram of hydrocracking product with MCT81-500

on differences in the content of carbon chains, as summarized in Table 3.

GC-MS data for liquid products from the cracking process are divided into several fractions, including biogasoline (C_5-C_{12}), kerosene (C_{12}-C_{15}), diesel (C_{16}-C_{18}), and wax fractions (> C_{18}). The percentage of each product

Table 3. Chemical composition of hydrocracking product with MCT81-500

Chemical compound	Fraction	R. Time	Area (%)	Height (%)	A/H
n-Heptane	C_7	1.41	0.66	1.20	0.71
1-*n*-Heptene	C_7	1.46	0.99	1.50	0.85
n-Octane	C_8	1.54	6.37	9.89	0.84
1-Octene (CAS) Caprylene	C_8	1.64	7.50	11.18	0.87
2-Octene, (Z)- (CAS) (*Z*)-2-Octene	C_8	1.68	2.41	2.96	1.06
2-Octene (CAS) Oct-2-ene	C_8	1.72	1.34	1.50	1.15
n-Nonane	C_9	1.80	12.01	15.44	1.01
3-Propylcyclopentene,	C_5	1.88	0.50	0.25	2.61
(*Z*)-Cycloheptene	C_7	1.92	0.38	0.43	1.16
n-Non-1-ene	C_9	1.99	13.40	14.74	1.18
2-Nonene	C_9	2.07	1.92	1.86	1.34
Propylcyclohexane	C_6	2.24	1.61	0.98	2.14
1-Ethylcyclohexene	C_6	2.28	1.13	0.86	1.69
Decane	C_{10}	2.33	4.98	5.49	1.18
7-Methyl-bicyclo[2,2,1]heptane	C_8	2.37	0.80	0.66	1.57
9,12,15-Octadecatrienal	C_{20}	2.40	0.28	0.28	1.31
Bis(cyclopent-2-enyl)	C_{11}	2.47	0.68	0.63	1.40
3,10-Dioxa-tricyclo	C_{12}	2.49	0.44	0.44	1.31
trans-1-Ethenyl-2-methylcyclohexane	C_6	2.53	0.28	0.20	1.82
Cyclopentane	C_5	2.59	0.95	0.53	2.32
1-Decene	C_{10}	2.71	10.16	7.91	1.66
Cyclooctene	C_8	2.75	10.14	8.52	1.54
cis-3-Decene	C_{10}	2.86	2.04	1.87	1.42
Pentalene	C_8	2.97	2.49	1.46	2.22
4,5-Nonadiene	C_9	3.07	0.63	0.27	3.02
n-Butylcyclohexane	C_6	3.16	0.79	0.37	2.77
Hexanal	C_6	3.21	0.77	0.37	2.71
Undecane	C_{11}	3.37	1.77	1.31	1.75
Cyclodecene	C_{10}	3.44	0.43	0.26	2.16
4-Cyclopropylcyclohexene	C_9	3.47	0.47	0.32	1.88
6-Methyl-bicyclo[4.2.0]octan-7-ol	C_9	3.59	1.10	0.55	2.58
Ethylbenzene	C_6	3.90	0.79	0.26	3.93
1-Dodecene	C_{12}	4.12	3.48	2.19	2.06
2-Undecene	C_{11}	4.42	2.69	1.40	2.50
1-Butylcyclohexane	C_6	4.57	0.67	0.35	2.48
1-Undecene	C_{11}	4.68	1.16	0.69	2.20
1,2-Dimethylbenzene, (CAS) *o*-Xylene	C_6	5.14	0.55	0.29	2.45
Propylbenzene (CAS) *n*-Propylbenzene	C_6	5.77	0.27	0.14	2.39
3-Methylcyclohex-3-en-1-one	C_7	12.23	0.57	0.25	2.93
Pentadecane	C_{15}	17.69	0.18	0.08	2.86
Benzaldehyde	C_7	18.18	0.24	0.12	2.49

fraction is calculated from the resulting peak area to obtain the data summarized in Fig. 9.

Based on Fig. 9, the percentage of the product fraction from the thermal and hydrocracking processes with a catalyst shows significantly different results. The thermal cracking performed showed that the biogasoline and kerosene fractions obtained were relatively low. On the other hand, the selectivity of catalysts MCT21-500, MCT41-500, and MCT81-500 in hydrocracking palm oil resulted in a dominant gasoline fraction of 76.81, 83.54, and 92.24 wt.%, respectively. This is indicated that mesoporous silica catalysts can capture the free fatty acid (FFA) as well as it can make cracking into shorter hydrocarbons, as shown in Fig. 10. Based on GC-MS analysis, the resulting molecules are hydrocarbons and oxygenated compounds containing fatty acids and alcohols. This fact confirms that the mechanism of the cracking reaction of palm oil includes the hydrogenation of triglycerides into fatty acids, hydrogenation of fatty acids into aldehydes and alcohols, and deoxygenation of fatty acids through decarbonylation, decarboxylation, and hydrodeoxygenation reactions [35,39-40].

Hydrocarbon molecules can be formed directly from fatty acids through decarboxylation by releasing carbon dioxide molecules (CO_2) to produce alkanes (saturated hydrocarbons) and decarbonylation by releasing carbon monoxide (CO) and water (H_2O) to produce alkenes (unsaturated hydrocarbons). Both of these reactions mostly occur in Lewis acid sites [41],
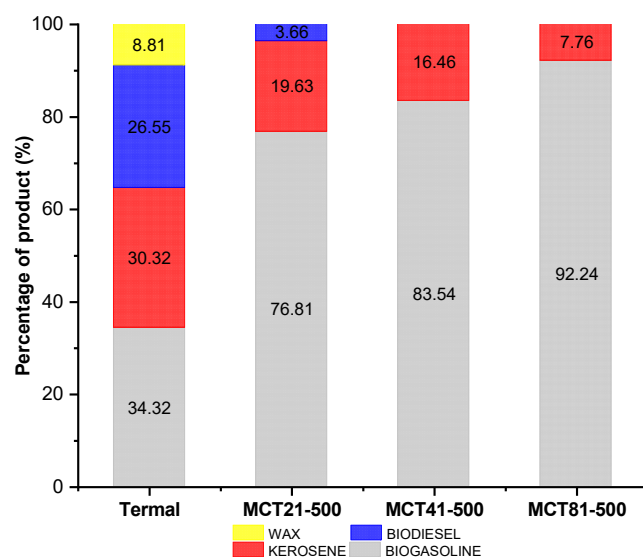

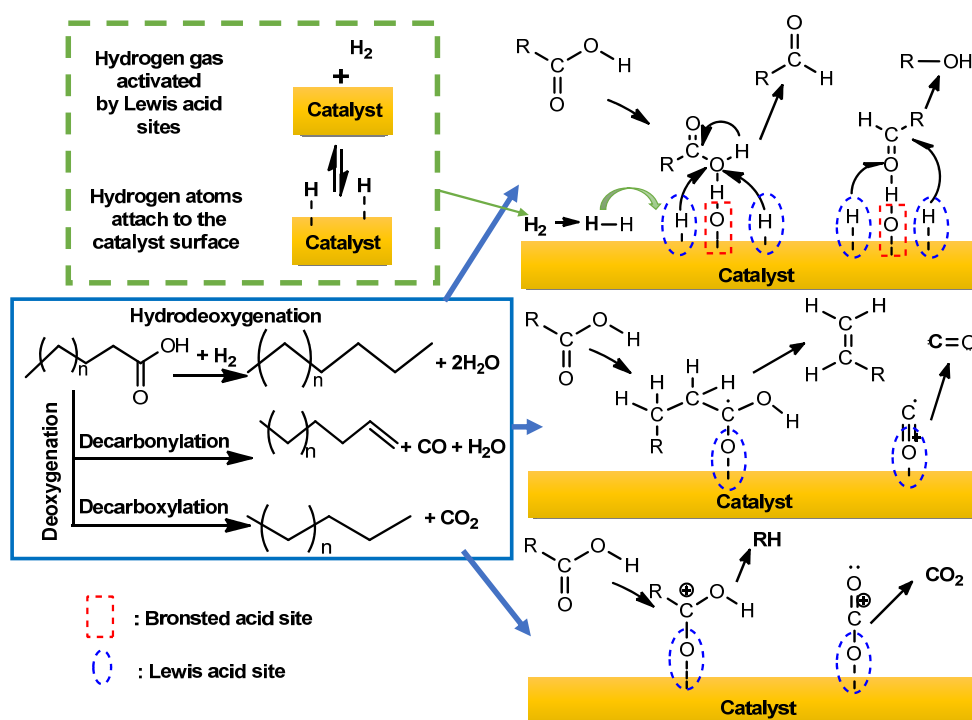**Fig 9.** Product fraction percentages produced from the hydrocracking process using various catalysts

Fig 10. Mechanism of hydrocracking of palm oil with MCT catalyst

Indones. J. Chem., 2023, 23 (2), 285 - 297

293

with the hydrocarbons formed being C_{15} (kerosene group) and C_{17} (diesel group).

On the other hand, hydrocarbons below C_{15} and oxygenated compounds are formed by hydrocracking reactions with the hydrogenation of hydrogen gas activated by Lewis acid sites [42]. The reactions mostly take place at Brønsted acid sites. In this study, this hydrogenation mechanism dominates the reaction as evidenced by the GC-MS results produced in Fig. 8. It is suggested that alcohol molecules are formed through the hydrogenation of fatty acids into aldehydes and then converted into alcohols through further hydrogenation of aldehydes. In addition, the hydrogenation reaction is more detailed theoretically, as shown in Fig. 11 [43]. In heterogeneous catalysts, the hydrogen forms surface hydrides (M–H) from which the hydrogen can be transferred to the chemically adsorbed substrate. H_2 undergoes heterolytic association to form H^+H^- [44]. In heterogeneous catalysts, hydrogen forms surface hydrides (M-H) from which hydrogens can be transferred to the chemisorbed substrate. Hydrogen gas is activated by Lewis acid sites to produce alkanes (or hydrogen) and carbenium ions n-C_iH_{2i} [42]. While Bronsted acid plays a role in cracking carbon chains so that a reaction mechanism occurs, forming the hydrocarbons below C_{15} and oxygenated compounds by hydrocracking reactions, protonated to the secondary alkyl carbenium ions (n-$C_iH_{2i+1}^+$) [43]. The mesoporous silica catalyst protonates the alkane chains to produce a transition state of

carbonium ions which collapse to give alkanes (or hydrogen) and the carbenium ions n-C_iH_{2i} dissociate from the Lewis acid site and diffuse to the Brønsted acid site where they are protonated into secondary alkyl carbenium ions, n-$C_iH_{2i+1}^+$. Carbenium ion is a reactive intermediate that can undergo several conversions, such as rearrangement of the framework and breaking of the C-C bond. The β-scission fragment is a smaller alkyl carbenium ion and an alkene. In the case of β-slicing n-$C_iH_{2i+1}^+$, a primary carbenium ion is formed, which is energetically unfavorable. Therefore, the n-alkyl carbenium ion undergoes an exclusively skeletal rearrangement, in which a single branched alkyl carbenium ion, iso-$C_iH_{2i+1}^+$, is formed. If there is an efficient desorption mechanism from the acid site, single-branched alkenes, iso-C_iH_{2i}, are released and diffuse to the Lewis acid site where they are hydrogenated to become single-branched alkanes, iso-C_iH_{2i+2}. These are prime products that are observed with low conversions [43].

Thus, the type of catalyst in the hydrocracking of used palm oil can affect the selectivity of liquid products to the gasoline fraction that is produced. The results showed that the use of mesoporous silica in the catalytic activity test increased the amount of product from the gasoline fraction (C_5-C_{12}). The percentage of product using mesoporous silica catalyst MCT81-500 showed an increase in the product of the gasoline fraction associated with an increase in crystallinity and a decrease
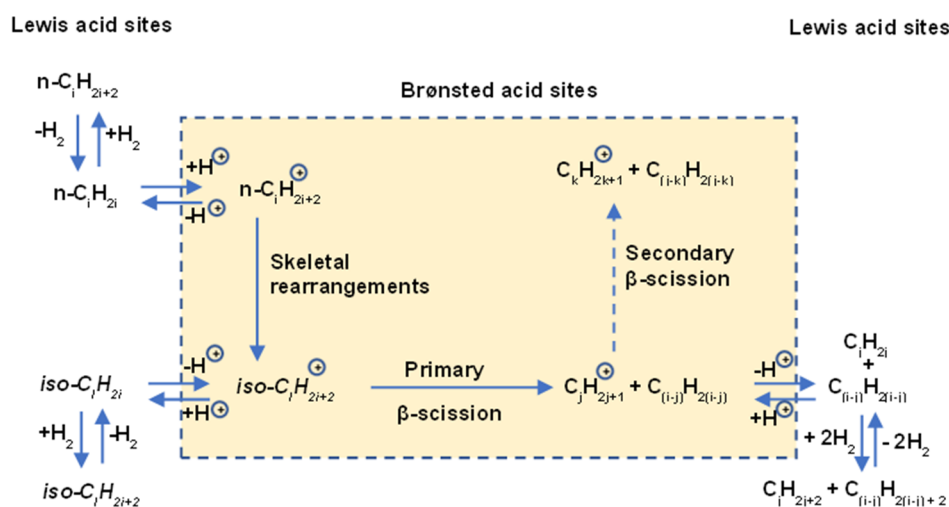

Fig 11. Mechanism of hydrogenation reaction on hydrocracking by MCT catalyst

in matrix content in the synthesis of this material. Based on this description, MCT81-500 with an H_2 gas flow rate of 20 mL/min, a catalyst/feed ratio of 1:100, and a time of 1 h was found to be the most optimal to produce the best gasoline fraction. MCT81-500 material has been successfully used as a catalyst for the process of hydrocracking palm oil into biogasoline.

The concentration of TEOS used affects the amount of silica yield obtained. The greater the amount of TEOS used, the greater the silica product obtained. This result is in accordance with reference [45], where TEOS concentration strongly influences the formation of a mesoporous material network. A higher amount of TEOS showed an irregular mesostructured, while a lower amount was insufficient to form a mesoporous structure [46]. The particle size increased with an increasing number of TEOS. Table 2 shows an increase in the pore diameter of the MCT81-500 sample, thereby increasing the availability of the active surface, allowing an increase in the ability of mesoporous silica for hydrocracking used palm oil into the biogasoline. This is shown by the catalyst with a larger average pore diameter in Table 2, which has a higher absorbed volume intensity in Fig. 6. This results in an increasing number of active catalyst surface sites that play a role in the hydrogenation process in hydrocracking. The more hydrogenation processes in hydrocracking that occur, as shown in Fig. 10 and 11, the more gasoline products will be produced compared to other products. This is because of the reasons explained in the reaction mechanism that products with molecules below C_{15}, especially gasoline and oxygenated compounds, are formed more in the hydrogenation process through the Lewis acid site and Bronsted acid site. In addition, the larger pore volume does not impede the diffusion process, so the hydrogenation reaction runs faster. Thus, the gasoline product will be dominant with a large porous catalyst and more surface-active sites in the hydrogenation reaction.

In addition, by looking at the hydrocracking mechanism involving Lewis acid sites and Brønsted acid sites on the catalyst, further studies related to acidity and the effect of pH on the optimal performance of hydrocracking reactions become important parameter studies. Higher catalyst acidity will show better potential for use as a catalyst that requires an acidic site, such as hydrocracking [35]. The presence of H^+ will help the process of protonation of *n*-alkanes to become the secondary alkyl carbenium ions (n-$C_iH_{2i+1}^+$) so that more product conversions can be produced.

■ CONCLUSION

Synthesis of mesoporous silica catalyst and its activity and selectivity in the hydrocracking of used palm oil has been carried out. The use of CTAB as a matrix in the production of mesoporous silica has been successfully achieved, as evidenced by the crystallinity, and increase in the pore size distribution of silica in the meso dimension. This study showed that the highest selectivity for the biogasoline fraction (92.24 wt.%) was produced by the MCT81-500 catalyst at an H_2 gas flow rate of 20 mL/min with a catalyst/feed ratio of 1:100 (w/w) for 1 h. Material MCT81-500 was successfully used as a catalyst in the process of hydrocracking palm oil into hydrocarbons (biogasoline).

■ ACKNOWLEDGMENTS

■ AUTHOR CONTRIBUTIONS

All authors have contributed equally.

■ REFERENCES

[1] Yaqoob, H., Teoh, Y.H., Goraya, T.S., Sher, F., Jamil, M.A., Rashid, T., and Yar, K.A., 2021, Energy evaluation and environmental impact assessment of transportation fuels in Pakistan, *Case Stud. Chem. Environ. Eng.*, 3, 100081.

[2] Altarazi, Y.S.M., Abu Talib, A.R., Yu, J., Gires, E., Abdul Ghafir, M.F., Lucas, J., and Yusaf, T., 2022, Effects of biofuel on engines performance and emission characteristics: A review, *Energy*, 238, 121910.

[3] Kabeyi, M.J.B., and Olanrewaju, O.A., 2022, Biogas production and applications in the sustainable energy transition, *J. Energy*, 2022, 8750221.

[4] Hanafi, S.A., Elmelawy, M.S., El-Syed, H.A., and Shalaby, N.H., 2015, Hydrocracking of waste cooking oil as renewable fuel on NiW/SiO₂-Al₂O₃ catalyst, *J. Adv. Catal. Sci. Technol.*, 2 (1), 27–37.

[5] Dik, P.P., Danilova, I.G., Golubev, I.S., Kazakov, M.O., Nadeina, K.A., Budukva, S.V., Pereyma, V.Y., Klimov, O.V., Prosvirin, I.P., Gerasimov, E.Y., Bok, T.O., Dobryakova, I.V., Knyazeva, E.E., Ivanova, I.I., and Noskov, A.S., 2019, Hydrocracking of vacuum gas oil over NiMo/zeolite-Al₂O₃: Influence of zeolite properties, *Fuel*, 237, 178–190.

[6] Sarvi, M.N., Budianto Bee, T., Gooi, C.K., Woonton, B.W., Gee, M.L., and O'Connor, A.J., 2014, Development of functionalized mesoporous silica for adsorption and separation of dairy proteins, *Chem. Eng. J.*, 235, 244–251.

[7] Tao, Y., Ju, E., Ren, J., and Qu, X., 2015, Bifunctionalized mesoporous silica-supported gold nanoparticles: Intrinsic oxidase and peroxidase catalytic activities for antibacterial applications, *Adv. Mater.*, 27 (6), 1097–1104.

[8] Lee, Y.C., Dutta, S., and Wu, K.C.W., 2014, Integrated, cascading enzyme-/chemocatalytic cellulose conversion using catalysts based on mesoporous silica nanoparticles, *ChemSusChem*, 7 (12), 3241–3246.

[9] Gao, W., Hu, Y., Xu, L., Liu, M., Wu, H., and He, B., 2018, Dual pH and glucose sensitive gel gated mesoporous silica nanoparticles for drug delivery, *Chin. Chem. Lett.*, 29 (12), 1795–1798.

[10] Lai, S.M., Lai, H.Y., and Chou, M.Y., 2014, A facile approach for the tunable wormlike or ordered pore morphology of mesoporous silica: Effect of catalyst types and polyethylene glycol, *Microporous Mesoporous Mater.*, 196, 31–40.

[11] Hikosaka, R., Nagata, F., Tomita, M., and Kato, K., 2016, Adsorption and desorption characteristics of DNA onto the surface of amino functional mesoporous silica with various particle morphologies, *Colloids Surf., B*, 140, 262–268.

[12] Ng, T.N., Chen, X.Q., and Yeung, K.L., 2015, Direct manipulation of particle size and morphology of ordered mesoporous silica by flow synthesis, *RSC Adv.*, 5 (18), 13331–13340.

[13] Knežević, N., and Durand, J.O., 2015, Large pore mesoporous silica nanomaterials for application in delivery of biomolecules, *Nanoscale*, 7 (6), 2199–2209.

[14] Wei, J., Sun, Z., Luo, W., Li, Y., Elzatahry, A.A., Al-Enizi, A.M., Deng, Y., and Zhao, D., 2017, New insight into the synthesis of large-pore ordered mesoporous materials, *J. Am. Chem. Soc.*, 139 (5), 1706–1713.

[15] Wang, X., Zhang, Y., Luo, W., Elzatahry, A.A., Cheng, X., Alghamdi, A., Abdullah, A.M., Deng, Y., and Zhao, D., 2016, Synthesis of ordered mesoporous silica with tunable morphologies and pore sizes via a nonpolar solvent-assisted Stöber method, *Chem. Mater.*, 28 (7), 2356–2362.

[16] Zhang, W., Zuo, H., Cheng, Z., Shi, Y., Guo, Z., Meng, N., Thomas, A., and Liao, Y., 2022, Macroscale conjugated microporous polymers: controlling versatile functionalities over several dimensions, *Adv. Mater.*, 34 (18), 2104952.

[17] Luo, W., Zhao, T., Li, Y., Wei, J., Xu, P., Li, X., Wang, Y., Zhang, W., Elzatahry, A.A., Alghamdi, A., Deng, Y., Wang, L., Jiang, W., Liu, Y., Kong, B., and Zhao, D., 2016, A micelle fusion-aggregation assembly approach to mesoporous carbon materials with rich active sites for ultrasensitive ammonia sensing, *J. Am. Chem. Soc.*, 138 (38), 12586–12595.

[18] Yuan, K., Che, R., Cao, Q., Sun, Z., Yue, Q., and Deng, Y., 2015, Designed fabrication and characterization of three-dimensionally ordered arrays of core-shell magnetic mesoporous carbon microspheres, *ACS Appl. Mater. Interfaces*, 7 (9), 5312–5319.

[19] Gao, M., Zeng, J., Liang, K., Zhao, D., and Kong, B., 2020, Interfacial assembly of mesoporous silica-based optical heterostructures for sensing applications, *Adv. Funct. Mater.*, 30 (9), 1906950.

[20] Nasir, T., Herzog, G., Hébrant, M., Despas, C., Liu, L., and Walcarius, A., 2018, Mesoporous silica thin

films for improved electrochemical detection of paraquat, *ACS Sens.*, 3 (2), 484–493.

[21] Liu, Y., Shen, D., Chen, G., Elzatahry, A.A., Pal, M., Zhu, H., Wu, L., Lin, J., Al-Dahyan, D., Li, W., and Zhao, D., 2017, Mesoporous silica thin membranes with large vertical mesochannels for nanosize-based separation, *Adv. Mater.*, 29 (35), 1702274.

[22] Upare, D.P., Park, S., Kim, M.S., Kim, J., Lee, D., Lee, J., Chang, H., Choi, W., Choi, S., Jeon, Y.P., Park, Y.K., and Lee, C.W., 2016, Cobalt promoted Mo/beta zeolite for selective hydrocracking of tetralin and pyrolysis fuel oil into monocyclic aromatic hydrocarbons, *J. Ind. Eng. Chem.*, 35, 99–107.

[23] Upare, D.P., Park, S., Kim, M.S., Jeon, Y.P., Kim, J., Lee, D., Lee, J., Chang, H., Choi, S., Choi, W., Park, Y.K., and Lee, C.W., 2017, Selective hydrocracking of pyrolysis fuel oil into benzene, toluene and xylene over CoMo/beta zeolite catalyst, *J. Ind. Eng. Chem.*, 46, 356–363.

[24] Munir, D., and Usman, M.R., 2016, Synthesis and characterization of mesoporous hydrocracking catalysts, *IOP Conf. Ser.: Mater. Sci. Eng.*, 146, 012007.

[25] Williams, S., Neumann, A., Bremer, I., Su, Y., Dräger, G., Kasper, C., and Behrens, P., 2015, Nanoporous silica nanoparticles as biomaterials: Evaluation of different strategies for the functionalization with polysialic acid by step-by-step cytocompatibility testin, *J. Mater. Sci.: Mater. Med.*, 26 (3), 125.

[26] Porrang, S., Davaran, S., Rahemi, N., Allahyari, S., and Mostafavi, E., 2022, How advancing are mesoporous silica nanoparticles? A comprehensive review of the literature, *Int. J. Nanomed.*, 17, 1803–1827.

[27] Huo, Q., Margolese, D.I., and Stucky, G.D., 1996, Surfactant control of phases in the synthesis of mesoporous silica-based materials, *Chem. Mater.*, 8 (5), 1147–1160.

[28] Lai, C.Y, 2014, Mesoporous silica nanomaterials applications in catalysis, *J. Thermodyn. Catal.*, 5 (1), 1000e124.

[29] Lu, M., Liu, X., Li, Y., Nie, Y., Lu, X., Deng, D., Xie, Q., and Ji, J., 2016, Hydrocracking of bio-alkanes over Pt/Al-MCM-41 mesoporous molecular sieves

for bio-jet fuel production, *J. Renewable Sustainable Energy*, 8 (5), 053103.

[30] Nurmalasari, N., Trisunaryanti, W., Sutarno, S., and Falah, I., 2016, Mesoporous silica impregnated by Ni and NiMo as catalysts for hydrocracking of waste lubricant, *Int. J. ChemTech Res.*, 9 (9), 607–614.

[31] Yang, L., Wu, H., Jia, J., Ma, B., and Li, J., 2017, Synthesis of bimodal mesoporous silica with coexisting phases by co-hydrothermal aging route with P123 containing gel and F127 containing gel, *Microporous Mesoporous Mater.*, 253, 151–159.

[32] Wijaya, K., Saputri, W.D., Aziz, I.T.A., Wangsa, W., Heraldy, E., Hakim, L., Suseno, A., and Utami, M., 2021, Mesoporous silica preparation using sodium bicarbonate as template and application of the silica for hydrocracking of used cooking oil into biofuel, *Silicon*, 14 (4), 1583–1591.

[33] Sirajudin, N., Jusoff, K., Yani, S., Ifa, L., and Roesyadi, A., 2013, Biofuel production from catalytic cracking of palm oil, *World Appl. Sci. J.*, 26 (26), 67–71.

[34] Tambun, R., Gusti, O.N., Nasution, M.A., and Saptawaldi, R.P., 2017, Biofuel production from palm olein by catalytic cracking process using ZSM-5 catalyst, *JBAT*, 6 (1), 50–55.

[35] Salamah, S., Trisunaryanti, W., Kartini, I., and Purwono, S., 2021, Hydrocracking of waste cooking oil into biofuel using mesoporous silica from Parangtritis beach sand synthesized with sonochemistry, *Silicon*, 14 (7), 3583–3590.

[36] Liang, J., Liang, Z., Zou, R., and Zhao, Y., 2017, Heterogeneous catalysis in zeolites, mesoporous silica, and metal–organic frameworks, *Adv. Mater.*, 29 (30), 1701139

[37] Guillet-Nicolas, R., Bérubé, F., Thommes, M., Janicke, M.T., and Kleitz, F., 2017, Selectively tuned pore condensation and hysteresis behavior in mesoporous SBA-15 silica: Correlating material synthesis to advanced gas adsorption analysis, *J. Phys. Chem. C*, 121 (44), 24505–24526.

[38] Trisunaryanti, W., Triyono, T., Falah, I.I., Siagian, A.D., and Marsuki, M.F., 2018, Synthesis of Ce-mesoporous silica catalyst and its lifetime

determination for the hydrocracking of waste lubricant, *Indones. J. Chem.*, 18 (3), 441–447.

[39] Schreiber, M.W., Rodriguez-Nino, D., Gutiérrez, O.Y., and Lercher, J.A., 2016, Hydrodeoxygenation of fatty acid esters catalyzed by Ni on nano-sized MFI type zeolites, *Catal. Sci. Technol.*, 6 (22), 7976–7984.

[40] Istadi, I., Riyanto, T., Khofiyanida, E., Buchori, L., Anggoro, D.D., Sumantri, I., Putro, B.H.S., and Firnanda, A.S., 2021, Low-oxygenated biofuels production from palm oil through hydrocracking process using the enhanced Spent RFCC catalysts, *Bioresour. Technol. Rep.*, 14, 100677.

[41] Istadi, I., Riyanto, T., Buchori, L., Anggoro, D.D., Gilbert, G., Meiranti, K.A., and Khofiyanida, E., 2020, Enhancing Brønsted and Lewis acid sites of the utilized spent RFCC catalyst waste for the continuous cracking process of palm oil to biofuels, *Ind. Eng. Chem. Res.*, 59 (20), 9459–9468.

[42] Li, Y., Hou, C., Jiang, J., Zhang, Z., Zhao, C., Page, A.J., and Ke, Z., 2016, General H_2 activation modes for Lewis acid-transition metal bifunctional catalysts, *ACS Catal.*, 6 (3), 1655–1662.

[43] Weitkamp, J., 2012, Catalytic hydrocracking— Mechanisms and versatility of the process, *ChemCatChem*, 4 (3), 292–306.

[44] Aireddy, D.R., and Ding, K., 2022, Heterolytic dissociation of H_2 in heterogeneous catalysis, *ACS Catal.*, 12 (8), 4707–4723.

[45] Wang, D.K., and da Costa, J.C.D., 2018, "Silica, Template Silica and Metal Oxide Silica Membranes for High Temperature Gas Separation" in *Advanced Materials for Membrane Fabrication and Modification*, Eds. Gray, S., Tsuru, T., Cohen, Y., and Lau, W.J., CRC Press, Boca Raton, Florida, 231–274.

[46] Chiang, Y.D., Lian, H.Y., Leo, S.Y., Wang, S.G., Yamauchi, Y., and Wu, K.C.W., 2011, Controlling particle size and structural properties of mesoporous silica nanoparticles using the Taguchi method, *J. Phys. Chem. C*, 115 (27), 13158–13165.